able to show that, with the same coupling parameter, the rotational distribution of the fragment would broaden and shift to higher N'' values as the available energy increases. The same type of effect is seen in the experimental distributions in Figure 2.

The rotational distributions for the $v'' = 1$ also exhibit the same type of behavior as the $v'' = 0$ level. They in fact have similar impact parameters indicating that the same type of anisotropy is involved in the excited-state potential function. It appears that the difference that is observed in the vibrational energy is due to excitation of a slightly different region of the potential energy surface. If our interpretation of the branching between ground- and excited-state atoms is correct, then even when the molecule dissociates to give Br atoms in the excited state the fractional energy that appears in rotation is about the same as it is when ground-state atoms are produced. All of these suggest that the anisotropy in the excited-state potential curve is the controlling factor for these rotational distributions. It also may mean that any differences that are observed is just the result of forming the excited molecule on slightly different parts of the excited potential surface. Given the potential curves of the ground and excited state one might expect to get quantitative agreement between theory and experiment.

Conclusions

The nascent quantum state distributions of CN fragments produced in the photolysis of BrCN between 193 and 248 nm have been measured. The rotational distribution of the CN fragment broadens and shifts to higher energies with increases in available energy, which is in accord with recent theoretical predictions,[13] based upon an excited-state potential surface that has a large coupling coefficient between the translational and rotational motion.

At the lower energies and longer wavelengths, the observed rotational distribution for $CN(v''=0)$ is bimodal, indicating that there may be a shift in the photolysis mechanism when the wavelength of photolysis is changed. We have postulated that this bimodality is due to the simultaneous production of $Br(^2P_{1/2})$ and $Br(^2P_{3/2})$ atoms though it may be due to other effects. Houston and his group have shown that in the 266-nm photodissociation of ICN a bimodal rotational distribution can be obtained via nonadiabatic interactions on a single surface.[24] At the other wavelengths in the A continuum, where photodissociation has been studied, they needed at least three surfaces to reproduce all of the experimental data.[25] It is clear from their work and the work reported here that additional studies will have to be done on BrCN to obtain a full understanding of the photodissociation process.

The impact parameters for the photodissociation process were derived from the observed rotational distribution. The impact parameters are the same for all photolysis wavelengths between 190 and 266 nm if the bimodal distributions are identified with the production of Br atoms in the $^2P_{1/2}$ and $^2P_{3/2}$ states.

Vibrational excitation, contrary to rotation, decreases with available energy. The observed distribution indicates that there is weak coupling between vibrational and translational motion. The observed vibrational excitation has been explained in terms excitation of the hot bands of BrCN, namely those molecules in the 100 and/or the 110 state.

Acknowledgment. This work was supported by the Office of Naval Research. J.A.R. was supported by NASA under grant No. NAGW-446. I.A.M. acknowledges the support of the SOHIO Corp. J.H. was partially supported by NSF grant CHE8219255. We thank the referees and R. Schinke for their comments.

(24) Goldfield, E. M.; Houston, P. L.; Ezra, G. S. *J. Chem. Phys.* **1986**, *84*, 3120.
(25) Marinelli, W. J.; Sivakumar, N.; Houston, P. L. *J. Phys. Chem.* **1984**, *88*, 6685.

Collisional Quenching of $CH_3O(A^2A_1)$

Paul J. Wantuck,* Richard C. Oldenborg, Steven L. Baughcum, and Kenneth R. Winn

Chemistry Division, Los Alamos National Laboratory, Los Alamos, New Mexico 87545
(Received: September 10, 1986; In Final Form: December 29, 1986)

Room temperature rate constants for collisional quenching of $CH_3O(A^2A_1)$ have been measured for 20 collision partners. Methoxy radicals are produced by 248-nm photolysis of CH_3ONO and the $CH_3O(A^2A_1)$ is produced by exciting the A–X transition using a pulsed dye laser. Rate constants are determined by monitoring the time-resolved fluorescence signal as a function of quenching gas pressure. The experimental quenching cross sections are best correlated in terms of the CH_3O–collision partner interaction well depth. Reasonable correlation is observed for 15 quenching gases, but several exceptions are apparent. A similar trend in collision partner quenching efficiency for $OH(A^2\Sigma^+)$ and $CH_3O(A^2A_1)$ is noted and discussed.

I. Introduction

The methoxy radical (CH_3O) is known to be an important intermediate species in combustion reaction systems. In addition, photochemical reactions involving CH_3O are of importance to chemical processes in the atmosphere. Accurate, direct measurements of the reaction rate constants of methoxy radicals with various atmospheric and combustion system species are of particular interest and are generally not available. The reactions of CH_3O with O_2,[1,2] NO,[3] and NO_2[4] have been studied by the laser-induced fluorescence (LIF) technique. In all cases, the methoxy concentration was monitored by the fluorescence emission from the radical following excitation of A^2A_1–X^2E vibronic transitions with a dye laser beam probe. The LIF technique represents a highly sensitive, state-selective method of monitoring the concentration of the methoxy radical. The sensitivity of the technique is a function of the radiative lifetime of the excited state, the quantum efficiency for fluorescence, and the rate at which the excited state is quenched by various collision partners. Many room temperature reactions involving the methoxy radical proceed at relatively slow rates and measurement of these reaction rates with an LIF technique requires high concentrations of reactant.

(1) Gutman, D.; Sanders, N.; Butler, J. E. *J. Phys. Chem.* **1982**, *86*, 66.
(2) Lorenz, K.; Rhasa, D.; Zellner, R.; Fritz, B. *Ber. Bunsen-Ges Phys. Chem.* **1985**, *89*, 341.
(3) Sanders, N.; Butler, J. E.; Pasternack, L. R.; McDonald, J. R. *Chem. Phys.* **1980**, *48*, 203.
(4) McCaulley, J. A.; Anderson, S. M.; Jeffries, J. B.; Kaufman, F. *Chem. Phys. Lett.* **1985**, *115*, 180.

0022-3654/87/2091-3253$01.50/0

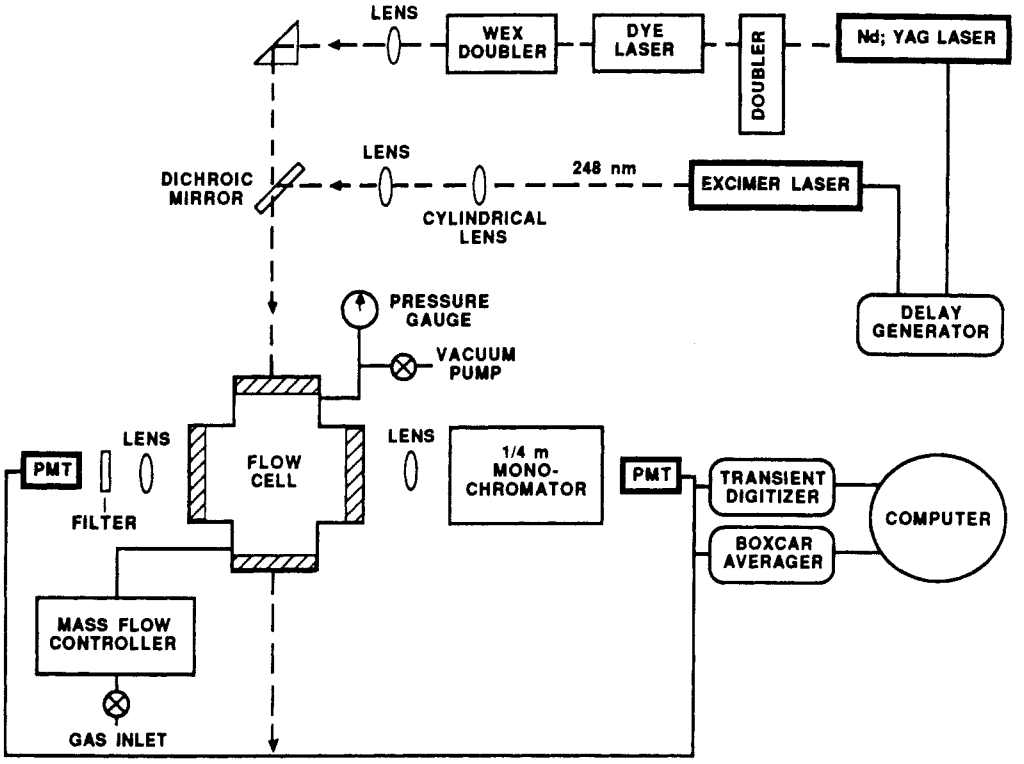

Figure 1. Optical schematic for the quenching experiments using a laser photolysis/LIF probe technique.

The sensitivity of the LIF technique will then depend strongly on the quenching rate. For example, Sanders et al.[3] using an LIF detection scheme, could not measure the room temperature reaction rate of methoxy with CO and have reported only an upper limit for the rate ($<8 \times 10^{-15}$ cm^3 molecule^{-1} s^{-1}). The reactions of CH_3O with CH_4 and O_2 have been studied in this laboratory.[5] At room temperature, the reaction rate for $CH_3O + O_2$ has been determined to be $(2.1 \pm 0.2) \times 10^{-15}$ cm^3 molecule^{-1} s^{-1}, a value in good agreement with results reported by other investigators.[1,2] However, the slow reaction rate of methoxy with methane, together with the efficient quenching of the CH_3O (A^2A_1) fluorescence emission by CH_4, limits the rate constant determination to an upper limit value of 10^{-15} cm^3 molecule^{-1} s^{-1}.

To assess the use of the LIF diagnostic for studying reactions involving the methoxy radical and for potential applications to in situ diagnostics, quenching rate constants are useful. Previous quenching studies of $CH_3O(A^2A_1)$ are limited. Ohbayashi et al.[6] established quenching rate constants from studies of the methoxy radical emission generated subsequent to flashlamp photolysis of CH_3ONO. Sanders et al.[3] estimated methoxy A-state quenching rate constants for some hydrocarbon species during their study of the $CH_3O + NO$ reaction.

In this paper we report measurements of room temperature $CH_3O(A^2A_1)$ quenching rate constants and their corresponding calculated cross sections for 20 collision partners. A combined laser photolysis/laser-induced fluorescence technique is used to perform these measurements.

II. Experimental Section

The methoxy radical is produced by photolyzing methyl nitrite (CH_3ONO) with a 248-nm (KrF) laser pulse. $CH_3O(A^2A_1)$ is produced by exciting on the A–X transition with a pulsed dye laser. The temporal evolution of the resulting fluorescence signal is measured as a function of the quenching gas concentration and then analyzed to determine a quenching rate constant.

A diagram of the apparatus used in these experiments is shown in Figure 1. The photolysis source is a Lambda Physik EMG 102 rare gas halide excimer laser operating on KrF at 248 nm. The probe laser wavelengths are generated with a Quanta Ray Nd:YAG laser-pumped dye laser. The excimer laser is pulsed at a 1-Hz repetition rate. To minimize detection of scattered excimer laser light, the dye laser is delayed 10 μs after the excimer laser pulse. To ensure that there is no influence of vibrational relaxation on $CH_3O(A^2A_1)$ quenching, CH_3O quenching studies are performed by monitoring the total fluorescence emission following excitation to both the (A^2A_1, $v_3' = 0 \leftarrow X^2E$, $v_3'' = 0$) transition at 316.4 nm and the (A^2A_1, $v_3' = 4 \leftarrow X^2E$, $v_3'' = 0$) transition at 292.8 nm. The 316.4-nm light is obtained by first pumping the DCM dye with the frequency-doubled output from the Nd:YAG laser. The resulting dye laser output is then frequency doubled to generate the desired probe laser wavelength. The 292.8-nm light is obtained in a similar manner by using the Kiton Red dye. The excimer and probe laser beams are introduced collinearly into the reaction cell. The size of the excimer beam is approximately 3 × 3 mm at the cell's center while the probe laser beam is focussed down to approximately 1 mm in diameter at the same location. The excimer and dye laser fluences are typically 0.14 and 1.7 J/cm^2, respectively.

For the quenching study, the total LIF signal resulting from methoxy radical excitation at 292.8 and 316.4 nm is imaged through 305- and 320-nm long-pass filters, respectively (Schott WG-305 and 320), onto the photocathode of a RCA 7265 gated photomultiplier tube. The photomultiplier signal is amplified and sent to a Tektronix R7912 transient digitizer. The processed signal is then recorded and analyzed with an interfaced NOVA/Data General Eclipse computer system. The processed signal represents the average temporal evolution of the fluorescence decay. Typically, 100 fluorescence decay traces are averaged for each quenching gas pressure setting.

For obtaining excitation and fluorescence spectra, the LIF signal is focussed onto the 2-mm-wide entrance slit of a 0.25-m Jarell-Ash monochromator. The output from the monochromator is monitored by a RCA 31034 photomultiplier tube. The signal is amplified and sent to a PAR Model 162 boxcar averager. As with the quenching experiments, the processed signal is recorded on a Data General NOVA 3 computer and then transferred to another computer (Data General Eclipse) for later analysis.

Quenching measurements are made by using two gas cell conditions hereafter referred to as flowing and static. With the flowing method, the methyl nitrite precursor, argon diluent, and

(5) Wantuck, P. J.; Oldenborg, R. C.; Baughcum, S. L.; Winn, K. R., manuscript in preparation.
(6) Ohbayashi, K.; Akimoto, H.; Tanaka, I. *J. Phys. Chem.* **1977**, *81*, 798.

quenching gas are continuously flowed through the cell. The various quenching gases and argon diluent are mixed in a high vacuum, gas handling system, enter the cell through a port located at its base, and flow vertically through the observation region. The argon diluent serves to translationally relax the methoxy radical photofragments. The precursor, premixed with argon (1% CH_3ONO in Ar), is introduced through an inlet at the bottom of the cell. Flow rates, for all gases, are measured and regulated by calibrated Tylan mass flow controllers. Gas flow through the cell is sufficient to assure that a fresh sample of CH_3ONO is present in the monitored volume for each successive laser shot, yet is essentially static when compared to the time scale of the quenching reaction. The bulk flow velocity in the cell is on the order of 5 cm/s. The cell windows are kept free of contaminants by flowing a steady stream of argon (≈10% of the total flow) over their internal surface.

The quenching effects of some gases like krypton and xenon are measured in the static condition, i.e., gases are added to a cell isolated from the pumping system. No window purge is operated during these experiments. Upon completion of a fluorescence decay measurement, the cell is pumped out and refilled with a fresh gas mix. For both gas cell conditions, cell pressure is monitored by various MKS Baratron pressure sensors.

The CH_3ONO and total argon pressure is, for the flowing condition, maintained at 2 mTorr and 25 Torr, respectively, and for the static case kept at 2 mTorr and 5 Torr. Quenching rate constants determined by using the flowing and static methods are, for the same quenching gas, essentially equivalent (≤5% difference).

The methyl nitrite precursor is synthesized following a procedure similar to that utilized by Gray and Style.[7] A mixture consisting of concentrated H_2SO_4 and distilled H_2O is slowly added to a solution of $NaNO_2$, CH_3OH, and distilled H_2O. The evolving gaseous methyl nitrite is carried by a N_2 stream and condensed in an ethanol slush trap. Further invacuo purification of the product is achieved by several passes through a multitrap distillation system. The final product is stored in a stainless steel cylinder and maintained at −196 °C.

Twenty quenching gases are utilized in this study. With the exception of CF_3H and CH_3ONO, which are obtained from in-house synthesis (<1% contaminants), all gases are commercial samples and utilized without further purification: Ar (99.99%), Kr (99.995%), Xe (99.995%), H_2 (99.999%), N_2 (99.99%), CO (99.9%), NO (99.9%), O_2 (99.99%), CO_2 (99.99%), CH_4 (99.99%), CH_3F (99.0%), CF_4 (99.7%), C_2H_4 (99.99%), SF_6 (99.5%), C_2H_6 (99.99%), C_3H_8 (99.97%), n-C_4H_{10} (99.9%), and i-C_4H_{10} (99.99%).

III. Results

A. Spectroscopy. The A^2A_1–X^2E electronic spectra of the methoxy radical have been studied and recorded by several investigators.[6,8,9] As a means of verifying the production and presence of the methoxy radical in our system, both laser-induced fluorescence excitation spectra and emission spectra resulting from various A–X transitions were recorded for comparison with established spectra. The LIF excitation spectra of CH_3O for the $\nu_3 = 0 \leftarrow 0$ and $4 \leftarrow 0$ vibronic bands are shown in Figure 2. Lines corresponding to rovibronic transitions are evident. The maxima of the $0 \leftarrow 0$ and $4 \leftarrow 0$ bands lie at 316.4 and 292.8 nm, respectively, and are in good agreement with values established by Inoue et al.[8]

The fluorescence spectra of $CH_3O(A^2A_1)$, resulting from excitation at 316.4 and 292.8 nm, are presented in Figure 3. As observed by Inoue et al., the intensity distribution for the $(0 \leftarrow 0)$ fluorescence spectrum shows a smooth envelope with a maximum at the (0, 3) peak. The (0, 0) and (4, 0) peaks show artificially high intensity due to scattered light from the exciting dye laser. The structure of the $(4 \leftarrow 0)$ fluorescence spectrum

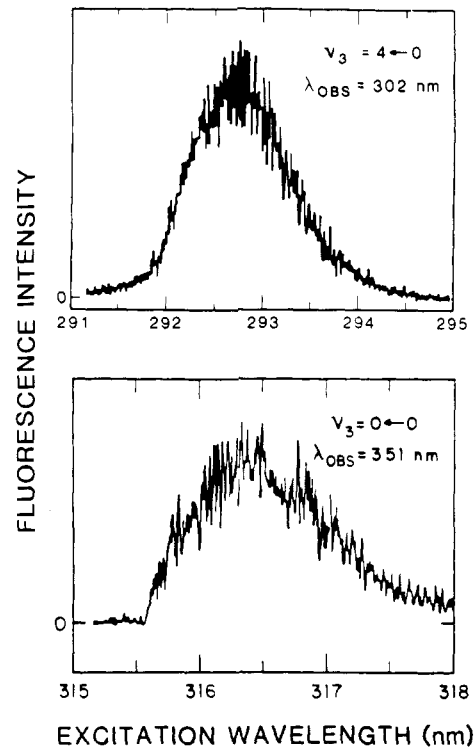

Figure 2. Laser-induced fluorescence excitation spectra of CH_3O showing the $\nu_3 = 0 \leftarrow 0$ and $4 \leftarrow 0$ vibronic bands.

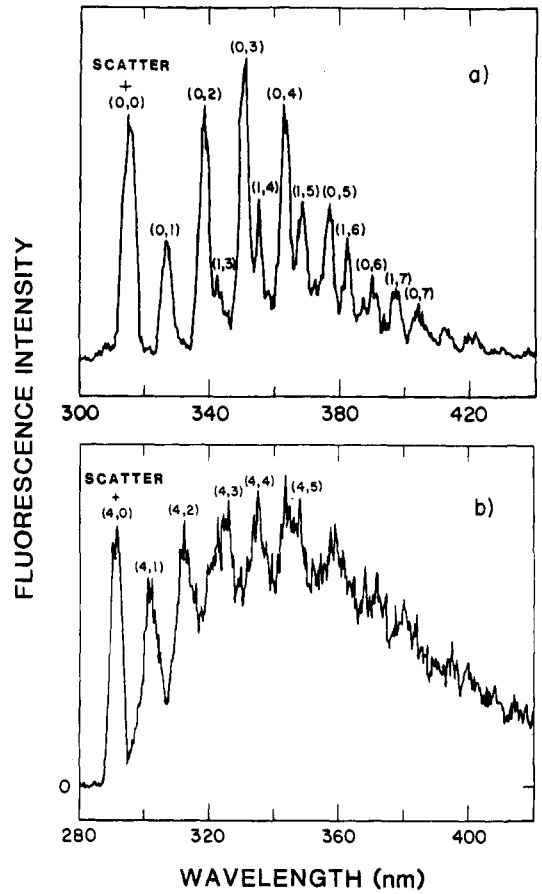

Figure 3. Laser-induced fluorescence spectra of CH_3O excited to (a) $\nu_3' = 0$ of $^2A_1$ at 316.4 nm, and (b) $\nu_3' = 4$ of $^2A_1$ at 292.8 nm. Scatter = extraneous contribution of scattered dye laser light.

is more diffuse although several of the main transition peaks can be identified. As opposed to the $\nu_3' = 0$ band, excitation on the $\nu_3' = 4$ band may lead to excitation of other combinations of vibronic states. This spectrum also matches that obtained by Inoue

(7) Gray, J. A.; Style, D. W. G. *Trans. Faraday Soc.* **1952**, *48*, 1137.
(8) Inoue, G.; Akimoto, H.; Okuda, M. *J. Chem. Phys.* **1980**, *72*, 1769.
(9) Inoue, G.; Akimoto, H.; Okuda, M. *Chem. Phys. Lett.* **1979**, *63*, 213.

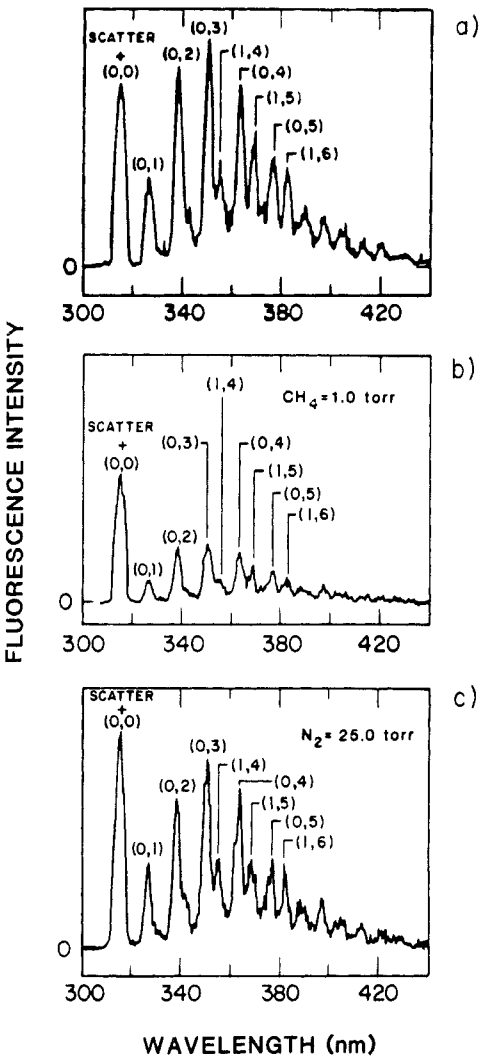

Figure 4. Effects of quenching by added CH_4 and N_2 on the LIF spectra from CH_3O (A–X) excited to $v_3' = 0$ of $^2A_1$ at 316.4 nm. Buffer gas pressure (argon) = 25 Torr, with (a) no additional gas, (b) 1.0 Torr of CH_4, (c) 25.0 Torr of N_2. Scatter = extraneous contribution of scattered dye laser light.

et al.[9] which they originally assigned as the (2 ← 0) spectrum, but later designated as corresponding to excitation of the $v_3' = 4$ band.[8]

B. Quenching. The fact that all of the CH_3O fluorescence occurs at longer wavelengths is beneficial to the quenching experiments since, with the use of long-pass filters, total fluorescence emission can be monitored, effectively decoupling the effects of vibrational relaxation.

The effects of quenching on the LIF spectra of CH_3O (A–X) excited on (0, 0) and (4, 0) bands are shown in Figures 4 and 5, respectively. Electronic quenching is evident in both spectra upon the addition of methane. In the presence of N_2, not only is a small amount of electronic quenching observed but the fluorescence peaks in the (4 ← 0) spectrum become somewhat less distinct as the effects of vibrational relaxation and redistribution become apparent. In contrast, the relative shape of the bands in the (0 ← 0) fluorescence spectrum are virtually unaltered by the addition of N_2.

The observed CH_3O fluorescence decay is single exponential for all quenching species investigated. A typical decay curve together with its logarithm and the best fit-single exponential are shown in Figure 6. This single-exponential type fluorescence decay permits the quenching rate constants to be determined by using the Stern–Volmer equation

$$1/\tau = 1/\tau_0 + \sum\{k_{RQ}[RQ]\} + k_Q[M] \qquad (1)$$

where τ represents the observed $CH_3O(A^2A_1)$ decay lifetime, τ_0 denotes the collision-free fluorescence lifetime, k_{RQ} is the bimolecular quenching rate constant for the species present other than the quencher M, namely RQ (i.e., Ar, CH_3ONO, CH_3O, and NO), and k_Q represents the bimolecular quenching rate constant for the species M. A plot of $1/\tau$ vs. pressure of M gives, as the intercept, the sum of the first two terms in eq 1, and the slope as k_Q. For these experiments, the intercept was essentially constant for all quenching species investigated. Since the precursor concentration was kept low and argon is a very inefficient quencher of $CH_3O(A^2A_1)$, the intercept is, to good approximation, a measure of the collision-free fluorescence lifetime, τ_0. The value of τ_0 was determined to be 2.2 ± 0.1 μs. This collision-free fluorescence lifetime is consistent with results reported by Inoue et al.[9] (1.5 μs), McCaulley et al.[4] (2.0 μs), and Ohbayashi et al.[6] (3.0 μs).

Representative Stern–Volmer type plots for CF_4, N_2 (inefficient quenchers), CH_4, and CO (efficient quenchers) are presented in Figure 7. The lines plotted through the points represent a best (least square-type) fit to the data. Quenching rate constants determined by using eq 1 and the corresponding quenching cross sections are listed in Table I for all the quenching species investigated. The quenching cross section, σ_Q, is defined by the relation $\sigma_Q = k_Q/v$, where v represents the average relative interaction velocity.

The observed quenching cross sections may be classified into two groups, i.e., efficient quenchers comprising all the hydrogen- and oxygen-containing species, and Xe, as well as the inefficient quenchers, namely the rare gases, N_2, CF_4, and SF_6. Both physical- and chemical-type quenching channels may be operating. Collision partners which might be expected to react with CH_3O, such as O_2 and CH_4, appear to be very efficient quenchers. For the inefficient quenchers, the Stern–Volmer plots are linear over the pressure ranges investigated [Kr (30 Torr), Ar (400 Torr), N_2 (300 Torr), SF_6 (100 Torr), CF_4 (60 Torr)]. As mentioned previously, $CH_3O(A^2A_1)$ quenching rates were determined following excitation of the radical to both the $v_3' = 0$ and 4 levels. Quenching rate constants established for excitation of both these vibronic levels for the quenching species CH_4, O_2, and CF_4 are displayed in Table II. Within experimental uncertainty, there is little if any difference in the observed quenching rate constants. This result is not surprising because by monitoring the broad-band

TABLE I: Room Temperature $CH_3O(A^2A_1)$ Quenching Rate Constants and Cross Sections

collision partner	k_Q, cm^3 molecule^{-1} s^{-1}	σ_Q, Å^2
Ar	$<3.5 \times 10^{-14}$	<0.006
Kr	$(9.2 \pm 0.1) \times 10^{-13}$	0.17 ± 0.01
Xe	$(7.7 \pm 0.6) \times 10^{-11}$	15.3 ± 1.3
H_2	$(5.6 \pm 0.1) \times 10^{-11}$	3.0 ± 0.1
N_2	$(9.0 \pm 0.2) \times 10^{-13}$	0.14 ± 0.01
CO	$(9.5 \pm 0.2) \times 10^{-11}$	14.5 ± 0.4
NO	$(6.9 \pm 1.6) \times 10^{-11}$	11 ± 3
O_2	$(2.5 \pm 0.2) \times 10^{-11}$	4.0 ± 0.3
CO_2	$(4.5 \pm 0.2) \times 10^{-11}$	7.7 ± 0.4
CH_4	$(1.05 \pm 0.07) \times 10^{-10}$	13.6 ± 0.9
CH_3F	$(8.9 \pm 0.5) \times 10^{-11}$	14.2 ± 0.8
CF_3H	$(1.4 \pm 0.2) \times 10^{-10}$	25 ± 4
CF_4	$(1.40 \pm 0.05) \times 10^{-13}$	0.027 ± 0.001
C_2H_4	$(1.5 \pm 0.2) \times 10^{-11}$	23 ± 3
CH_3ONO	$(4.2 \pm 0.2) \times 10^{-10}$	76 ± 3
SF_6	$(1.4 \pm 0.1) \times 10^{-14}$	0.0030 ± 0.0002
C_2H_6	$(6.8 \pm 0.3) \times 10^{-11}$	10.6 ± 0.4
C_3H_8	$(1.5 \pm 0.5) \times 10^{-10}$	25 ± 9
n-C_4H_{10}	$(3.2 \pm 0.3) \times 10^{-10}$	58 ± 6
i-C_4H_{10}	$(3.0 \pm 0.2) \times 10^{-10}$	54 ± 4

TABLE II: Room Temperature Quenching Rate Constants and Cross Sections following Excitation on the $v_3 = 0$ and 4 Vibronic Levels

species	v_3'	k_Q, cm^3 molecule^{-1} s^{-1}	σ_Q, Å^2
O_2	0	$(2.5 \pm 0.2) \times 10^{-11}$	4.0 ± 0.3
	4	$(2.7 \pm 0.2) \times 10^{-11}$	4.3 ± 0.3
CH_4	0	$(1.05 \pm 0.07) \times 10^{-10}$	13.6 ± 0.9
	4	$(1.09 \pm 0.05) \times 10^{-10}$	14.1 ± 0.7
CF_4	0	$(1.40 \pm 0.05) \times 10^{-13}$	0.027 ± 0.001
	4	$(1.32 \pm 0.04) \times 10^{-13}$	0.025 ± 0.001

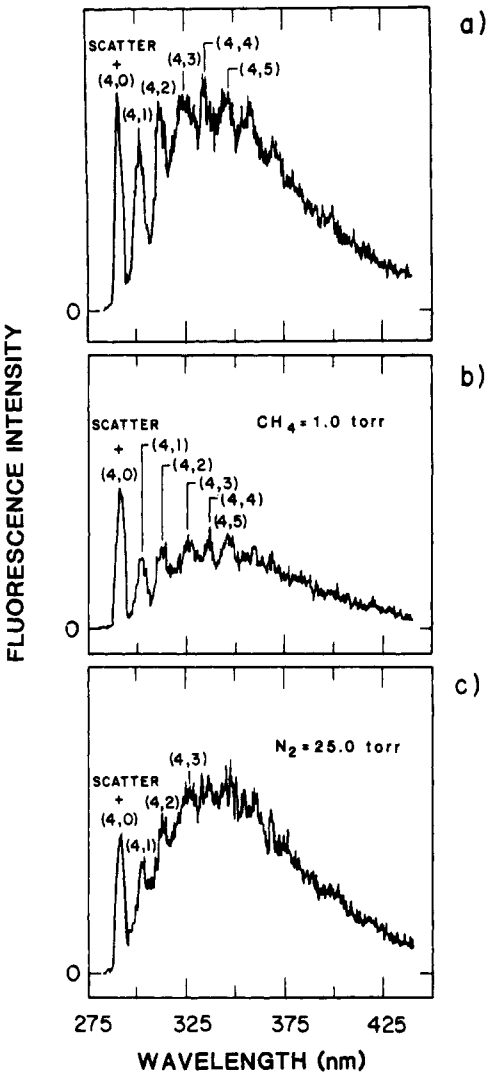

Figure 5. Effects of quenching by added CH_4 and N_2 on the LIF spectra from CH_3O (A–X) excited to $v_3' = 4$ of $^2A_1$ at 292.8 nm. Buffer gas pressure (argon) = 25 Torr, with (a) no additional gas, (b) 1.0 Torr of CH_4, (c) 25.0 Torr of N_2. Scatter = extraneous contribution of scattered dye laser light.

TABLE III: Comparison of $CH_3O(A^2A_1)$ Room Temperature Quenching Cross Sections Measured by Ohbayashi et al.[a] with Results of the Current Investigation[b]

collision partner	$\sigma(M)/\sigma(CO)^a$	$\sigma(M)/\sigma(CO)^b$
Ar	<0.01	<0.0004
Kr	0.11	0.01
Xe	1.4	1.06
H_2	0.25	0.21
N_2	0.01	0.01
CO	1.0	1.0
O_2	0.33	0.28
CO_2	0.65	0.53
CH_4	0.97	0.94
C_2H_6	2.0	0.73
C_3H_8	3.7	1.8
CH_3ONO	4.0	5.2

CH_3O fluorescence emission, only A-state electronic quenching rate constants are measured.

The quenching cross sections obtained in this study are compared in Table III with relative values measured by Ohbayashi et al.,[6] by normalizing the cross section values using the quenching cross section of CO. For most of the compared relative cross sections, reasonable agreement is noted. Sanders et al.[3] note that the $CH_3O(A^2A_1)$ quenching rates established during their investigation of the CH_3O + NO reaction are in qualitative agreement with relative rates extracted from the Ohbayashi data, and that methane, isobutane, ethylene, and propane are particularly efficient quenchers of $CH_3O(A^2A_1)$.

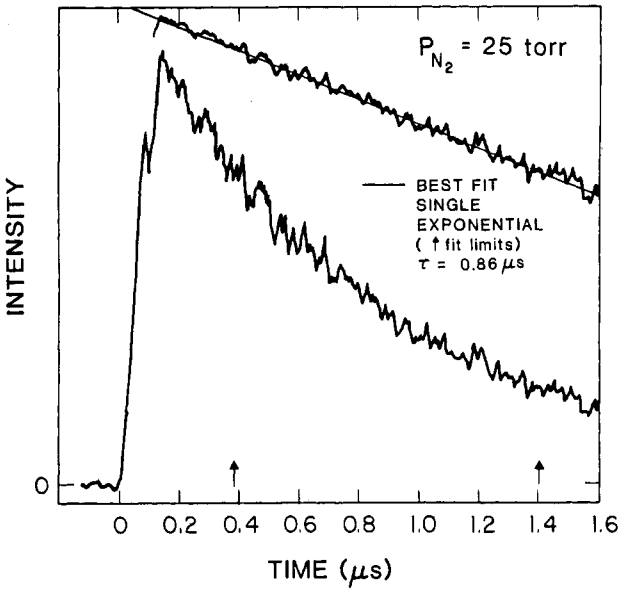

Figure 6. Typical fluorescence signal decay curve together with its logarithm and best-fit single exponential. Conditions: λ_{EXC} = 316.4 nm, P_{Ar} = 25 Torr, P_{N_2} = 25 Torr.

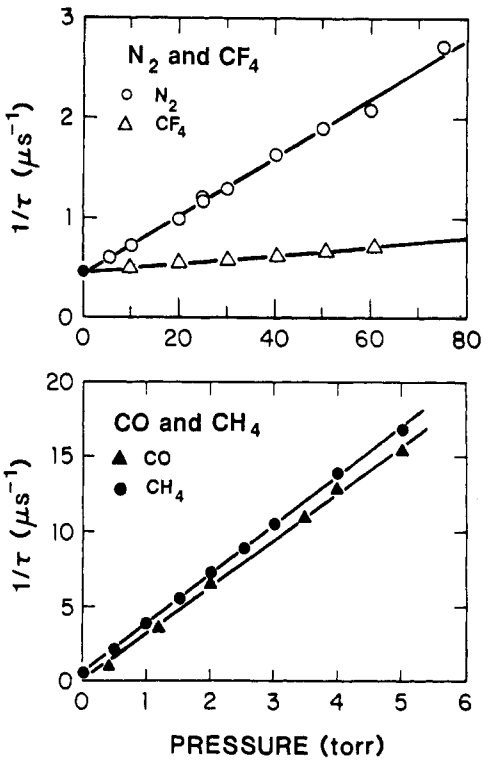

Figure 7. Stern–Volmer plots corresponding to eq 1 for the quenching species N_2, CF_4, CO, and CH_4.

C. Quenching Models. Several models have been proposed to correlate measured electronic quenching cross sections with parameters such as the ionization potential, polarizability, and collision diameter.[10-15] Correlation of some of these models with the observed $CH_3O(A^2A_1)$ quenching rate constants were attempted, but the results were generally unsuccessful. The model of Rössler,[10] which correlates quenching efficiency in terms of the

(10) Rössler, F. *Z. Phys.* **1935**, *96*, 251.
(11) Thayer, C. A.; Yardley, J. T. *J. Chem. Phys.* **1972**, *57*, 3992.
(12) Lin, H. M.; Seaver, M.; Tang, K. Y.; Knight, A. E. W.; Parmenter, C. S. *J. Chem. Phys.* **1979**, *70*, 5442.
(13) Holtermann, D. L.; Lee, E. K. C.; Nanes, R. *J. Chem. Phys.* **1982**, *77*, 5327.
(14) Selwyn, J. E.; Steinfeld, J. I. *Chem. Phys. Lett.* **1969**, *4*, 217.
(15) Asscher, M.; Haas, Y. *J. Chem. Phys.* **1985**, *76*, 2115.

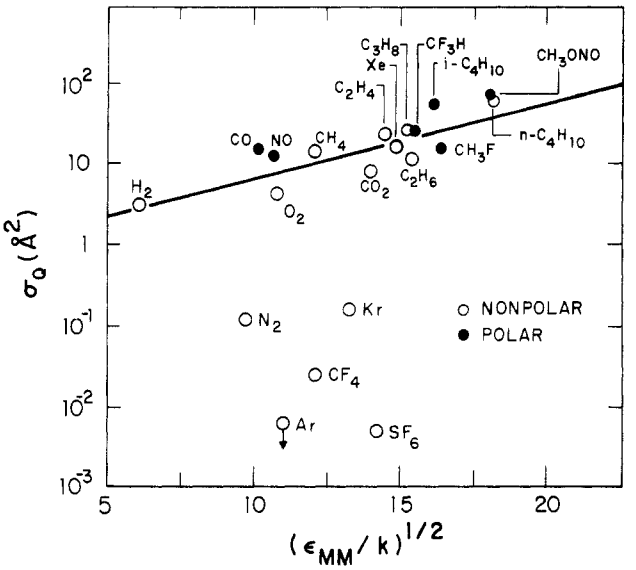

Figure 8. Measured quenching cross sections vs. the well-depth model parameter $(\epsilon_{MM}/k)^{1/2}$. Argon cross section represents an upper limit.

reduced mass and polarizability of the collision partner, was applied to the current quenching rate constant data, but as also observed by Ohbayashi,[6] did not provide a satisfactory correlation. The dispersion-force parameter used by Thayer and Yardley to correlate the collision-induced quenching of propynal[11] was also unsuccessfully applied to correlate the observed $CH_3O(A^2A_1)$ quenching rate constants. The best correlation is achieved when the experimental cross sections are compared in terms of the well-depth (collision complex) model proposed by Lin et al.[12] This model assumes that the quenching rate is dependent upon attractive forces between the excited species (A*) and the collision partner (M) and requires only that the collision complex be a transient pair. In this model, the quenching cross section is related to the intermolecular well depth between A* and M, ϵ_{A^*M}, by

$$\sigma_Q = C[\exp(\epsilon_{A^*M}/kT)] \quad (2)$$

where C represents a constant of the A* + M interaction, k denotes Boltzmann's constant, and T is the temperature. When the approximation proposed by Lin et al.,[12] namely $\epsilon_{A^*M} = (\epsilon_{A^*A^*}\epsilon_{MM})^{1/2}$, is used to calculate the A*–M interaction well depth, eq 2 becomes

$$\ln \sigma_Q = \ln C + \beta(\epsilon_{MM}/k)^{1/2} \quad (3)$$

where $\beta = (\epsilon_{A^*A^*}/kT^2)^{1/2}$, and ϵ_{MM} denotes the well depth for a M–M interaction. A plot of the room-temperature CH_3O (A^2A_1) quenching cross sections vs. the parameter $(\epsilon_{MM}/k)^{1/2}$ is shown in Figure 8. Values of ϵ_{MM} were obtained for all the quenching species investigated, except CH_3ONO, from a list compiled by Lin et al.[12] The well depth for CH_3ONO was estimated by using the empirical rule $\epsilon_{MM}/k = 1.15T_b$, where T_b is the boiling point.[16] It is apparent from Figure 8 that the well-depth model is not entirely successful in correlating the $CH_3O(A^2A_1)$ quenching cross sections. The experimental values of σ_Q for the quenching species Ar, Kr, N_2, SF_6, and CF_4 are conspicuously low. However, for the hydrogen- and oxygen-containing species (collision partners which might be expected to react with CH_3O) and Xe, the comparison of the quenching cross sections with the interaction well depth shows a reasonable correlation. The slope of the line, β, is equal to $0.23K^{-1/2}$ and the intercept value, C, equals 0.7. For the corresponding plot for the OH radical[17] (which exhibits characteristics similar to the methoxy radical[18]), β has a value of $0.19K^{-1/2}$ and C is equal to 1.8.

(16) Hirschfelder, J. O.; Curtiss, C. F.; Bird, R. P. *Molecular Theory of Gases and Liquids*; Wiley: New York, 1954; p 245.
(17) Fairchild, P. W.; Smith, G. P.; Crosley, D. R. *J. Chem. Phys.* **1983**, *79*, 1795.
(18) Brossard, S. D.; Carrick, P. G.; Chappell, E. L.; Hulegaard, S. C.; Engelking, P. C. *J. Chem. Phys.* **1986**, *84*, 2459.

TABLE IV: Comparison of Room Temperature $OH(A^2\Sigma^+)$ and $CH_3O(A^2A_1)$ Quenching Cross Sections[a]

quencher	OH $\sigma_Q(A^2\Sigma^+)$	CH_3O $\sigma_Q(A^2A_1)$
H_2	11.6[b], 9.2[c]	3
N_2	6.7[b], 4.0[c]	0.14
O_2	20.7[b], 18.7[c]	4.0
CF_4	<3[b]	0.025
SF_6	<3[b]	0.003
NO	47.7[b]	11.0
CO	49.6[b]	14.5
CO_2	69,[b] 57.4[c]	7.7
CH_4	34.4[b]	13.6
CF_3H	27.1[b]	25
C_2H_4	89.5[b]	23
C_2H_6	80.3[a]	10.6

[a] Units = Å^2. [b] Reference 19, $J = 0$ rotational level. [c] Reference 20.

Xenon is observed to be a relatively efficient quencher of $CH_3O(A^2A_1)$ when correlated by well depth. However, since the positions of the Ar and Kr quenching cross sections are well off the correlation line, the position of the Xe cross section on this line may be coincidental. The freon compounds, namely CF_4, CF_3H, and CH_3F, are observed to quench at different rates. The replacement of even one fluorine atom with a hydrogen atom dramatically increases the quenching efficiency of the excited methoxy radical. This alludes to the possibility that reaction channels make a significant contribution to the quenching process, or at least that the physical quenching channel can be significantly enhanced by chemical interactions between the colliding species. As noted previously, collision partners which might be expected to react with CH_3O, in this case the oxygen- and hydrogen-containing species, are efficient methoxy A-state quenchers. Several reactions are possible. Quenching of electronically excited methoxy (*) could occur through a hydrogen abstraction reaction

$$CH_3O^* + R \rightarrow CH_2O + RH \quad (4)$$

where one of the products is formaldehyde. A hydrogen addition reaction

$$CH_3O^* + RH \rightarrow CH_3OH + R \quad (5)$$

producing methanol also represents a possible quenching process. For the oxygen-containing species CO and NO, an additional chemical reaction route is possible, namely

$$CH_3O^* + RO \rightarrow CH_3 + RO_2 \quad (6)$$

The reaction of CH_3O^* with a species M can result in the formation of formaldehyde (CH_2O) via the decomposition reaction

$$CH_3O^* + M \rightarrow CH_2O + H + M \quad (7)$$

or the hydroxymethyl radical (CH_2OH) via the isomerization reaction

$$CH_3O^* + M \rightarrow CH_2OH + M \quad (8)$$

The physical quenching reaction

$$CH_3O^* + M \rightarrow CH_3O + M \quad (9)$$

represents an additional quenching process for CH_3O^*. Some insight as to which reactions may be operating as CH_3O^* quenching channels can be gained by considering quenching of the excited OH radical.

D. Comparison with OH. The methoxy radical is homologous to the OH radical and the A^2A_1–X^2E transition is analogous to the $A^2\Sigma^+$–$X^2\Pi$ transition of OH.[18] Inoue et al.[8] note that the A^2A_1 state is 31 540 cm^{-1} above the ground state for CH_3O, while the $A^2\Sigma^+$ state of OH is 32 683 cm^{-1} above the ground state. The radiative lifetime of $OH(A^2\Sigma^+)$ is 0.8 μs,[9] somewhat shorter than the measured fluorescence lifetime (2.2 μs) of $CH_3O(A^2A_1)$. Because the two radicals possess a certain degree of similarity it seems reasonable to compare, as well, the quenching cross sections of $OH(A^2\Sigma^+)$ with that of $CH_3O(A^2A_1)$. Quenching of $OH(A^2\Sigma^+)$ has been studied quite extensively. In recent inves-

tigations, Copeland et al.[19] and Copeland and Crosley[20] have measured room temperature OH quenching cross sections for a variety of collision partners and Fairchild et al.[17] have measured quenching rates for OH at elevated temperatures. The room temperature $OH(A^2\Sigma^+)$ quenching cross sections are listed along with cross sections established for $CH_3O(A^2A_1)$ in Table IV. The measured quenching cross sections for CH_3O are lower in all cases than the OH values. A similar trend is observed with the OH quenching rates, namely, efficient OH A-state quenchers are efficient CH_3O A-state quenchers. As with CH_3O, quenching rate measurements for OH obtained by using N_2 and SF_6 as well as CF_4 showed these species to be relatively inefficient quenchers. In addition, as with CH_3O, fair correlation is achieved when the $OH(A^2\Sigma^+)$ experimental quenching cross sections are compared in terms of the well-depth model.[17]

If we extend the similarity between OH and CH_3O quenching behavior to the reactions outlined in section IIIC, we can conclude that, since OH cannot isomerize or easily decompose, $CH_3O(A^2A_1)$ quenching through decomposition (reaction 7) or isomerization (reaction 8) reaction channels is probably of lesser importance. Therefore, quenching of $CH_3O(A^2A_1)$ proceeds through one or more of the remaining processes (reactions 4, 5, 6, or 9). A definitive determination of which process (or processes) is of importance to methoxy quenching would require monitoring of product species. Such an investigation is under consideration for future study.

Acknowledgment. This work was supported by the Morgantown Energy Technology Center (DOE) and was performed under the auspices of the Department of Energy. We thank Dr. Joe J. Tiee for useful discussions and Kenneth V. Salazar for his assistance in synthesizing the CH_3ONO.

(19) Copeland, R. A.; Dyer, M. J.; Crosley, D. R. *J. Chem. Phys.* **1985**, *82*, 4822.
(20) Copeland, R. A.; Crosley, D. R. *J. Chem. Phys.* **1986**, *84*, 3099.

Laser Multiphoton Ionization Dissociation Mechanisms from Comparison of the Wavelength-Dependent Laser Mass Spectra with That Predicted from the Breakdown Curves: 2,4-Hexadiyne

Diane M. Szaflarski, Eric L. Chronister, and M. A. El-Sayed*

Department of Chemistry and Biochemistry, University of California, Los Angeles, California 90024
(Received: October 17, 1986; In Final Form: January 30, 1987)

The mass peak intensity ratio of $C_4H_3^+$ to $C_4H_4^+$, the dominant fragment ion peaks in the low laser power mass spectrum of 2,4-hexadiyne, is studied at different picosecond laser wavelengths that are one-photon-resonant with the $^1B_2$ (S_2) excited state. It was found that the ratio correlates with the dependence on the internal energy of the parent ion predicted from the previously determined breakdown curves if one assumes that the internal energy (E^*) of the parent ion formed in the multiphoton absorption has an energy dependence on the laser wavelength used of the form $b + hc/\lambda$, where $b = 0.3$ eV. The form of this equation and the ability to obtain an agreement at different laser wavelengths with the results of the breakdown curve strongly support a ladder mechanism for the formation of both $C_4H_4^+$ and $C_4H_3^+$ by a two-photon ionization–three-photon dissociation process when a picosecond laser is used. The constancy of b when S_2 is excited at different laser wavelengths is briefly discussed in terms of the dynamics in S_2 and the statistical nature of the ionic dissociation process.

Introduction

Understanding the mechanisms of the interaction of pulsed lasers with matter is complicated by the fact that, at high light intensities, a certain mass fragment can be produced by a number of dissociation–ionization channels.[1,2] For example, a fragment ion can be formed by first ionizing the parent molecule which is followed by further photon absorption and dissociation (the ionic ladder mechanism). Alternatively, dissociation of the parent *molecule* could occur first which is followed by absorption and ionization of the fragment radicals (the ladder-switching mechanism). Adding to the complication of determining laser multiphoton ionization dissociation (MPID) mechanisms for many systems is the lack of information such as appearance potentials and breakdown curves for the different fragment ions.

A breakdown curve is a plot of the probability of forming a fragment ion as a function of the internal energy of the parent ion. Breakdown curves have traditionally been constructed with monoenergetic electron beams[3] or vacuum-UV photons[4] as ionization sources. Presently, several groups are studying breakdown curves by the photoion–photoelectron coincidence (PIPECO) technique,[5] as ions are detected in coincidence with zero kinetic energy electrons. PIPECO is used to determine the probability of forming different fragment ions as a function of the well-defined internal energy of the parent ion.

Previously, a two-color picosecond technique was developed[6] and applied to 2,4-hexadiyne[7] and 1,4-dichlorobenzene,[8] by which the time dependence of the different mass fragments is measured on the picosecond–nanosecond time scale. Assuming an ionic ladder mechanism, the time dependence of the mass fragments measures the energy redistribution times of the excited levels of the parent ion that are the precursors for the different fragment ions. When the mass peaks of the $C_4H_4^+$ and $C_4H_3^+$ fragments, the most intense mass peaks at low 266-nm laser intensity, were studied by this technique, a characteristic time of 20 ns was observed.[6] This agrees with the lifetime of the excited state of the parent ion located near the three 266-nm photon absorption level which was measured previously[9] by fluorescence decay of

(1) Gedanken, A.; Robin, M. B.; Kuebler, N. A. *J. Phys. Chem.* **1982**, *86*, 4096.
(2) Gobeli, D. A.; Yang, J. J.; El-Sayed, M. A. *Chem. Rev.* **1985**, *85*, 529.
(3) Chupka, W. A.; Kaminsky, M. *J. Chem. Phys.* **1961**, *35*, 1991.
(4) (a) Steiner, B.; Giese, C. F.; Inghram, M. G. *J. Chem. Phys.* **1961**, *34*, 189. (b) Murad, E.; Inghram, M. G. *J. Chem. Phys.* **1964**, *40*, 3263.
(5) (a) Dannacher, J. *Chem. Phys.* **1978**, *29*, 339. (b) Das, P. R.; Gilman, J. P.; Meisels, G. G. *Int. J. Mass. Spectrom. Ion Phys.* **1986**, *68*, 155. (c) Bunn, T. L.; Richard, A. M.; Baer, T. *J. Chem. Phys.* **1986**, *84*, 1986.
(6) Gobeli, D. A.; Morgan, J. R.; St. Pierre, R. J.; El-Sayed, M. A. *J. Phys. Chem.* **1984**, *88*, 178.
(7) Gobeli, D. A.; El-Sayed, M. A. *J. Phys. Chem.* **1985**, *89*, 1722.
(8) Szaflarski, D. M.; Simon, J. D.; El-Sayed, M. A. *J. Phys. Chem.* **1986**, *90*, 5050.
(9) Allan, M.; Maier, J. P.; Marthaler, O.; Kloster-Jensen, E. *Chem. Phys.* **1978**, *29*, 331.

0022-3654/87/2091-3259$01.50/0